

# Measuring the Effects of Scalar and Spherical Colormaps on Ensembles of DMRI Tubes

Jian Chen, *Member, IEEE*, Guohao Zhang, *Student Member, IEEE*,  
Wesley Chiou, David H. Laidlaw, *Fellow, IEEE*, and Alexander P. Auchs

**Abstract**—We report empirical study results on the color encoding of ensemble scalar and orientation to visualize diffusion magnetic resonance imaging (DMRI) tubes. The experiment tested six scalar colormaps for average fractional anisotropy (FA) tasks (grayscale, blackbody, diverging, isoluminant-rainbow, extended-blackbody, and coolwarm) and four three-dimensional (3D) directional encodings for tract tracing tasks (uniform gray, absolute, eigenmap, and Boy’s surface embedding). We found that extended-blackbody, coolwarm, and blackbody remain the best three approaches for identifying ensemble average in 3D. Isoluminant-rainbow coloring led to the same ensemble mean accuracy as other colormaps. However, more than 50% of the answers consistently had higher estimates of the ensemble average, independent of the mean values. Hue, not luminance, influences ensemble estimates of mean values. For ensemble orientation-tracing tasks, we found that the Boy’s surface embedding (greatest spatial resolution and contrast) and absolute color (lowest spatial resolution and contrast) schemes led to more accurate answers than the eigenmaps scheme (medium resolution and contrast), acting as the uncanny-valley phenomenon of visualization design in terms of accuracy.

**Index Terms**—Ensemble visualization, diffusion magnetic resonance imaging, quantitative validation, colormap.



## 1 INTRODUCTION

EXPLORATORY vector and tensor field visualizations studying regions of interest or a group of objects at a time [1] count on the human visual system to extract statistical information from features. Perceiving average or other statistical features from a group of similar items, called *ensemble perception* [2] [3], is a robust visual phenomenon studied largely in vision science that operates across a host of visual dimensions: size [4], orientation [5], position [6], motion [7], speed [8], number [9], identities [10], structures [11], and luminance [12].

The applicability of these vision science results to visualizations is anecdotal because of at least two methodological barriers between these two domains. Vision science studies are intended to capture static views, separate perception and cognition from interaction, and also separate domain-specific uses from visual stimuli. In contrast, in visual exploration these factors must be integrated. Additionally, spatial visualization features, such as continuity, symmetry, and clusters, may not be present in images.

Working in collaboration with brain scientists, we have recognized two main challenges for showing 3D diffusion magnetic resonance imaging (DMRI) tractography. The first is to support ensemble univariate representations. Scalars are commonly encoded in one-dimensional (1D) colormaps, e.g., showing fractional anisotropy (FA) measured at every voxel to quantify disease states [13]. Though univariate col-

oring has been extensively studied in two-dimensional (2D) data visualizations (see the excellent reviews by Zhou and Hansen [14] and Silva et al. [15]), 3D color ensembles may introduce constraints in three respects. First, the univariate schemes of luminance and hue combination that work well in 2D may not apply in 3D, since luminance contrast can belie color constancy and distort 3D shape perception due to lighting [16]. Second, shading prevents the use of dark colors [17] [18], thus reducing the number of differentiable color s.png. Third, interpreting ensembles may not require visually deriving individual values [3]. Since scientific data are often continuous, the human visual system may well optimize strategies for efficient visual detection [19].

The second challenge is showing spatial brain structural connectivities from tracts (often rendered as tubes). This task requires the viewer to visually segment collections of tracts of various directions. Szafir et al. call this type of task *ensemble subset extraction* [20]; Phadke et al. call it *attribute value exploration* [1]. DMRI tracts, unlike data in these studies are continuous in space and carry domain-specific attributes such as *symmetry* and *proximate regions* [21] [22]. As a result, novel tract colorings concerning *tract locality*, *angular uniformity*, and *spatial resolution* have been explored [22]. No design knowledge exists, however, to quantify the practicality of these spherical colormaps in visualization.

The present work addresses these two important challenges by first summarizing a set of ensemble tasks of *identification*, *localization*, *comparison*, and *association* (Fig. 1). We then examine two identification tasks by evaluating state-of-the-art coloring methods. Specifically, we answer the following questions: *How reliable are colormaps for deriving ensemble averages from 3D spatially distributed tracts? Which colormaps are applicable to ensemble average? Which is the most effective ensemble orientation extraction technique?*

Our work makes the following contributions.

- J. Chen is with the Computer Science and Engineering Department, The Ohio State University, OH 43210. E-mail: chen.8028@osu.edu.
- G. Zhang and W. Chiou are with the Department of Computer Science and Electrical Engineering, University of Maryland, Baltimore County, MD 21025. E-mail: {guohaozhang, wchiou1}@umbc.edu.
- D.H. Laidlaw is with Computer Science Department, Brown University, RI 02912. E-mail: dhl@cs.brown.edu.
- A.P. Auchs is with the Neurology Department at the University of Mississippi Medical Center, Jackson, MS 39216. E-mail: aachus@umc.edu.

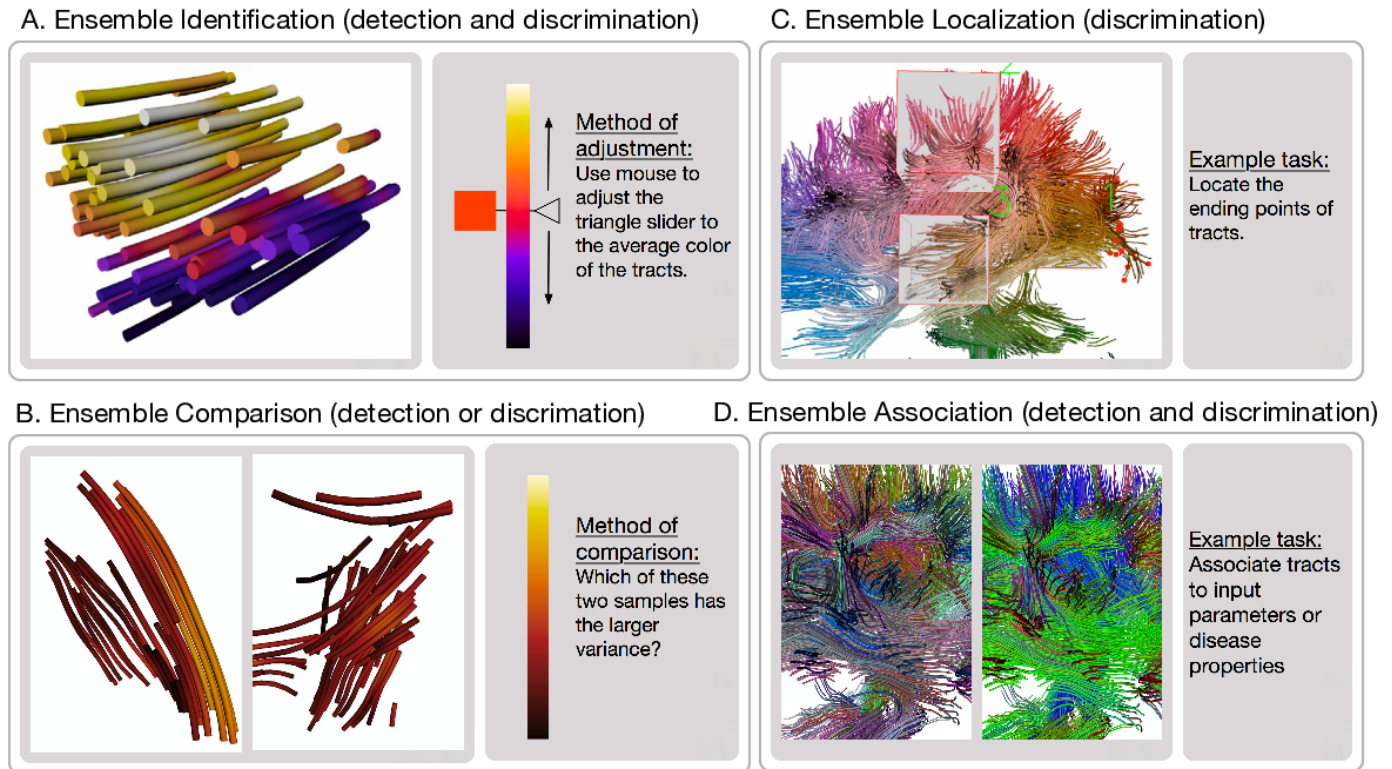


Fig. 1. Four Types of Ensemble Tasks and Example Methods for Testing Ensemble Visualization

- Formally proposes and expands ensemble visualization concepts inspired by vision science.
- Establishes new measurement metrics that permit us to match the data characteristics to color characteristics by analyzing data distributions.
- Suggests practical ensemble quantification methods to characterize visual dimensions.
- Derives some design recommendations for spatially continuous datasets for ensemble average and orientation discrimination.

## 2 TERMS AND RELATED WORK

Our work draws upon work related to (1) ensemble color representation results in vision science and (2) univariate and orientation representations in visualization. In this section, we broaden the definition of ensemble encoding in visualization and connect color theory to ensembles and relevant study results.

### 2.1 Ensemble Encodings: Definition

The *ensemble* concept in visualization often refers to a collection of datasets and is perhaps best known as ensemble simulation and uncertainty quantifications [23]. Ensemble has been broadly studied in vision science (e.g., [24]), where *ensemble representation* is used to explore how humans use statistical regularities in a group of similar objects to process information [25].

Our current work supports this recent broad perspective on the role of visual statistical processing and embraces

the idea that these visualization tasks, whether from ensemble simulations (statistical properties such as uncertainty [26] [27]) or not (e.g., overviews and detecting global features in flow fields [28] and areas or sets [29]), share the property that multiple measurements are combined to give rise to a higher-level statistical description.

Following this new human information processing perspective, we formalize **ensemble representation** as an umbrella term encompassing existing 3D visualization methods that demand the human visual system to derive statistical attributes from data. For example, correlated textures along vector fields help humans derive ensemble patterns to see flow movement; glyphs enable efficient visual assessment of “a chunk of flow” [30].

### 2.2 Color Ensembles

The study of **color ensemble representations** concerns how our visual system derives statistical information through visual processing of color features. Human vision can effectively process color ensembles, for example, to discount spectral variations and assign stable colors to objects to achieve consistent scene representation [31] and color constancy [16]. Color ensembles facilitate scalable visual inspection. Mauly and Franklin [32] study a series of uniformly colored circular elements ranging from 4 to 48 items subtended at 12, 20, and 28 just-noticeable differences (JNDs) and report that the accuracy was insensitive to changes in the number of elements in an ensemble. Only reaction time was longer for ensembles with more hues. Ensemble processing does not require focused attention to subsample of elements [12].

Dedicated human visual processing of ensemble colors may also exist [33]. In a 2D time-varying chart visualization, Correll et al. find that color is more effective than position for showing averages and distributions [34]; this is contradictory to classical design recommendations in which position is more accurate than color for quantitative comparisons, when ensemble is not required [35]. Also reliable average estimates can be made from two hues of red-blue, blue-green, and yellow green [36] and categorical boundaries can be accurately labelled for greenish-blue and bluish-green [37] and gray-scale alike textures [38].

These intriguing results on ensemble hues, mostly presented in vision science, seem to refute the idea that ensemble hues cannot be described in terms of magnitude but as qualitative experiences. They may be effective for ensemble averages and boundary detection when the data or hue variance is localized and small. In this work, we chose several multihue colormaps, such as extended-blackbody and coolwarm. We also use a reasonably good rainbow colormap, *aka* Kindlmann et al.'s isoluminant rainbow [39]. We compare these approaches against other univariate methods.

### 2.3 Univariate Coloring

The most influential color studies lie in univariate colormap design and characterizations (e.g., color harmony and categories [40] [41], metrics [42], and modeling [43]). Silva et al. [15] and Zhou and Hansen [14] summarize color characteristics important in univariate colormap design, such as *ordering* (colormaps must preserve the order in data), *separation* (different data must be perceived differently) [44], and *uniformity* (perceived differences in color must accurately reflect numerical data differences). Among these characteristics, uniformity is believed most important [45]. Rainbow colormap is believed to be poor at showing quantitative data because it lacks nearly all these attributes.

This design knowledge led us to adopt several univariate maps suggested by Moreland [18], including extended-blackbody (monotonic luminance and multihue), blackbody (perceptually uniform, monotonic luminance and multihue), coolwarm (perceptually uniform, two-hues and monotonic on each side), and diverging (two-hues and perceptually uniform and monotonic on each side). Some of them have also been incorporated in the popular 3D visualization tools VTK and Paraview. Since color ensembles by hues might be effective, we have also used Kindlmann et al.'s isoluminant rainbow [39] and used gray-scale as the baseline methods.

### 2.4 Vector and Tensor Field Evaluation

Pioneering 3D vector and tensor field studies have largely focused on univariate comparisons, such as vector speed between two locations [30], tracing a single tract [46], reading quantities at each sampling site [47], and showing depth and distances between adjacent occluded tracts [48] [49]. An exception is the study by Acevedo and Laidlaw [50] in which participants were to discriminate boundaries through a set of size-varying circles and must visually derive groups from visualization.

Borkin et al.'s work [51] closely resembles ours in terms of colormap comparisons to support seeing in 3D. That

study compares rainbow and diverging colormaps for detecting regions of heart diseases after projecting 3D artery flow patterns to 2D and finds that a rainbow colormap decreases detection rates [51]. The present work builds on these studies but expands the scope in two important ways: we measure more tasks to understand ensemble averages and direction discrimination, and our tasks are in 3D. We further formalize the task space in Chen et al. [52] for ensemble univariate and spherical direction discrimination.

### 2.5 Continuous Ensemble Spherical Colormaps

Knowledge about effective spherical colormap design is limited, despite their importance for showing tensor and vector fields. To show brain connectivity through tracts, Pajevic and Pierpaoli [21] use elegant solutions through extensive studies on *rotation* and *mirror symmetry*. The absolute values of the  $xyz$ -coordinates of the principal diffusion tensor eigenvectors are mapped directly to RGB colortriples. The advantages of this *absolute* approach include: (1) perceptual uniformity, (2) user familiarity with RGB colors associated with a vertebrate direction, (3) high contrast between vertebrate directions, and (4) four-way symmetry (left-right, dorsal-ventral, anterior-posterior, and antipodal.) Even though this absolute encoding approach provides a seemingly low-resolution view of tract orientation, our brain scientist collaborators suggest that this colormap dominates brain science because it conveys most important transverse, sagittal, and coronal directions.

Other solutions reveal patterns and increase spatial resolutions. Kindlmann et al. introduced a *hue-ball* approach and a barycentric map for direct volume rendering of tensor fields by assigning color and opacity based on the direction of the principal eigenvector and anisotropy type of the diffusion tensor [53]. An attractive characteristic of this approach is its high contrast between adjacent tracts: they are colored with bright, saturated colors spanning from red, yellow, green, cyan, blue to purple. Demiralp et al. [22] use *Boy's real projective plane immersion* to visualize the direction of brain tracts. This *Boy's surface* coloring possesses good *locality* and *contrast* by showing the finest details, and has the greatest *spatial resolution* of all spherical colormaps.

Vision science has studied multihue mainly as a pattern-segmentation mechanism for identifying structural variations. Maule et al. [54] suggest that there may be a functional limit to the amount of variance that can be rapidly encoded by summary statistics of set discriminations. Such set discriminations, though close to our orientation discrimination, can prescribe methods only for discrete clusters. No study exists to our knowledge to explore to what extent continuous spherical coloring of ensemble line field would be most beneficial. Our study compares four techniques to understand the effectiveness of ensemble orientation discriminations. Our hypothesis is largely driven by the vision science literature positioning that colormaps with higher resolution could improve the spherical color direction detection.

## 3 BRAIN DMRI DATA CHARACTERIZATION AND ENSEMBLE TASKS

This section first describes the data and task characterization by following Munzner's [55] data and task abstraction

method, and then presents our measurement method.

### 3.1 Brain DMRI Data Characterization

DMRI measures water diffusion as a second-order positive-definite tensor [56]. Water diffusion patterns have been analyzed comprehensively by brain scientists to study anatomical fibrous structures. Modern advances have extended to meta-analysis of brain cohorts [57]. Visualization design guidelines for understanding complex spatial structures have also been a recent focus [58], albeit disproportionately small in the amount of empirical work directly focused on evaluation. Preim et al. [59] have surveyed perceptually-motivated 3D visualization for medical imaging visualization, but focused on depth and shading. This challenge in coloring MRI datasets is often cited as a top visualization challenge [19].

The first and most reliable benchmark measurement is fractional anisotropy (FA) [60]. FA, a normalized scalar, measures the water diffusion patterns: a value of zero means that diffusion is isotropic, i.e., it is unrestricted in all directions (usually in gray matter); a value of one means that diffusion occurs only along one axis and is fully restricted (usually in white matter). Brain scientists are concerned with average FAs in regions containing a set of voxels or tracts. In this study, FAs are in the range of [0.2, 1] and average FAs are [0.25, 0.85].

Another important measurement is brain structural connectivities [52]. A continuous diffusion tensor field is first constructed from the measured DMRI data. Tracts are then computed at voxel sampling locations via tractography, a 3D technique for representing brain structural connectivity [61]. We terminate tract tracing when the FA value is less than 0.2. The tracts are depicted to show connectivity information. A group of tracts sharing similar orientations is called a bundle. Some studies use template-based approaches to derive and color tracts to show anatomical connectivity; others attempt to visualize the structures independent of templates. Our current work studies five major bundles labelled by our collaborators.

Several brain analysis tools and methods have supported colormaps. For example, DTI Studio lets users manually assign selected tracts a color as well as use the default randomly assigned colors for individual tracts [62]. 3D Slicer lets users select among a large variety of colormaps or customize their own for visualizing variables [63]. While these tools offer great flexibility, our results can give users more informed design choices among techniques and tools.

### 3.2 Ensemble Task Characterization

#### 3.2.1 Four Task Categories

We obtain the following measurable low-level tasks (Fig. 1). In each category, we separate detection (e.g., which is higher?) and discrimination (e.g., how much higher?) tasks inspired by Borgo et al. [64] and Zhao et al. [47], so as to address the goal of design for perceptually accurate visualizations.

- 1) *Ensemble identification* is performed when the goal is to read mean values or estimate the probability distributions of values from *similar* objects.

Some typical identification tasks are: what are the average FA values (Fig. 1(A))? Where is the boundary between regions of different anatomical structures? Do the two bundles belong to different groups? What is the average brain?

- 2) *Ensemble comparison* is useful to compare multiple ensembles or items or identify the most common outputs. Some example tasks are: are the left and the right hemispheres of CC different? If so, by how much? The task in Fig. 1(B) compares between diseases outcomes in cohorts.
- 3) *Ensemble localization* asks the viewer to find where a certain ensemble value or attribute is located within the data. Fig. 1(C) stresses visual lookup and asks where the lesion is in the brain. Where are regions of maximum and minimum mean FA values?
- 4) *Ensemble association* involves determining the associative relationships between or among *related* objects. Fig. 1(D) shows the average tracts computed from ensembles. Some example tasks are: which of these two average brains is associated with dementia? And at what state of the dementia? Using a simulator and after varying parameter A, what are the associated brain regions sensitive to these inputs, and what is the distribution of the changes among these output ensembles?

### 3.3 Metric

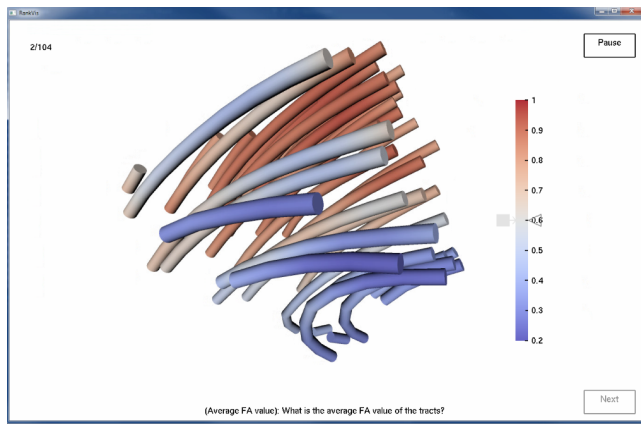
There are several considerations in measuring the ensemble representations. We divide the data or the colormap into bins to represent sub-regions. This is because a region of interest (ROI) in a spatial volume is likely to be localized to a group of data points. Also, we can associate the data distributions in each bin to color distributions in a colormap to understand colormap usefulness. For example, the spread or variance of the resulting distribution in each bin in a colormap reflects the ensemble average performance. The shape of the results also reflects the sensitivity of features or dimensions to the ensembles. Robust sensitivity to summary statistics will yield a narrow distribution. A function can also be fitted to the data to reveal sensitivity to the discriminative threshold to measure accuracy. In this work, for ensemble average we divide the input data into 12 bins and randomly sample the data such that each bin has a high-fidelity representation of the DMRI tract attributes. For orientation detection tasks, we follow past practice and measure the responses to spherical colormaps by randomly sampling the input.

## 4 ENSEMBLE EXPERIMENT FOR BRAIN DMRI VISUALIZATIONS

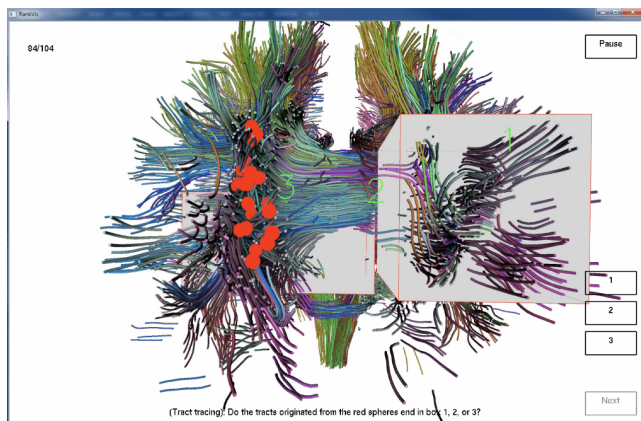
The objective here is to determine which ensemble colormaps are more accurate for showing DMRI datasets. We are particularly interested in the first task type, ensemble identification (of mean and orientation) (Section 3.2.1).

### 4.1 Hypotheses

Given our own experiences, our collaborators' subjective choices, and the literature, we have had five hypotheses when entering the experiment:



(a) Task 1: Ensemble Average



(b) Task 2: Ensemble Orientation

Fig. 2. Two Ensemble Identification Tasks in the Empirical Study. (a) What is the average value of the tracts? This example uses the diverging colormap. (b) Do the tubes originating from the red spheres end in box 1, 2 or 3? This example uses a Boy's surface colormap.

- H1 (rainbow hypothesis). For ensemble average, the isoluminant rainbow colormaps may be as accurate as uniform and monotonic luminance colormaps.
- H2 (multihue hypothesis). For ensemble average, multiple-hue colormaps can be effective for reading ensemble mean values.
- H3 (gray hypothesis). For ensemble average, baseline gray may have the worst accuracy for ensemble mean of scalar values.
- H4 (direction detection hypothesis). For ensemble orientation detection, higher spatial resolution can improve orientation accuracy.
- H5 (colorfulness hypothesis). Having color is better than baseline no-color uniform representation for identifying orientations.

## 4.2 Three-Dimensional Ensemble Tasks

### 4.2.1 Task 1: Ensemble Average (Discrimination task)

Figure 2(a) shows an example task in which participants were asked to label the average FA values of the brain areas sampled in a ROI. The participants indicate their answer for each task by dragging the slider on the screen to show the average color. The answers are evenly distributed along the 12 bins (see Section 5.3) so that participants are not biased.

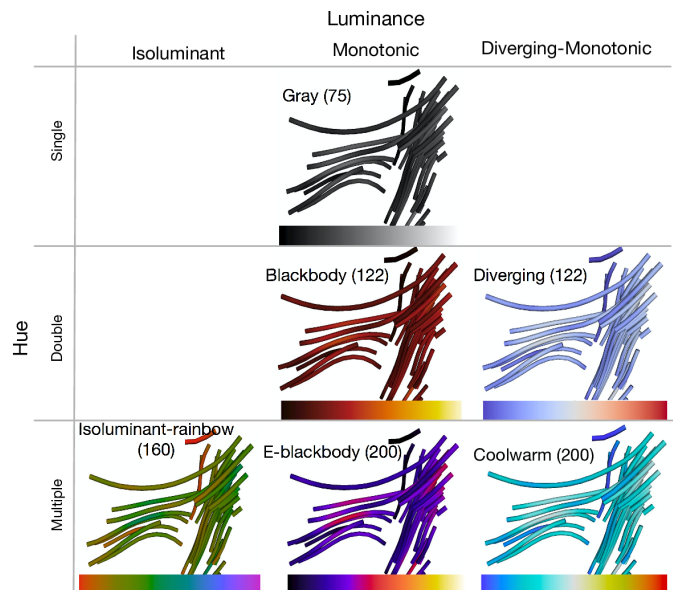


Fig. 3. Task 1's Six Univariate Colormaps. The numbers after colormap names are arc-lengths in the  $L^*A^*B^*$  color space.

### 4.2.2 Task 2: Ensemble Orientation (Detection task)

Figure 2(b) shows an example task in which participants were asked to find the one box among three in which the endpoints of the tracts marked by red spheres lay at one end of the tracts. Participants were told that the marked tracts in the same bundle followed the same orientation (anterior-posterior, dorsal-ventral, or left-right).

## 4.3 Choosing Ensemble Colormaps

### 4.3.1 Six Univariate Colormaps for Ensemble Average

Six univariate colormaps shown in Figure 3 are measured in task 1 (Ensemble Average).

These colormaps are chosen due to their popularity, relevance to our hypotheses, and our collaborators' recommendations. Arc-length is computed with CIEDE 2000 by summing the DeltaE values along the curve in the  $L^*A^*B^*$  color space [65]. All color interpolation is performed using linear interpolation in this  $L^*A^*B^*$  color space. The dark part is cut out to keep these values as close as possible for each hue condition. Appendix A shows the colormap profile in the  $L^*A^*B^*$  color space.

The *grayscale colormap* uses a single-hue and monotonic luminance with arc-length 75.

The *blackbody colormap* is a double-hue and monotonic luminance map inspired by the wavelengths of light from blackbody radiation. We use arc-length 122 instead of 145 to match that of the diverging map. We removed the dark end due to the low sensitivity to low luminance values.

The *diverging colormap* contains two hues and increases/decreases luminance monotonically with arc-length 122. The closer the color is to the center of the color map, the higher the luminance.

The *isoluminant-rainbow colormap* displays multihue rainbow with arc-length 160. It is isoluminant for the standard viewer, with the luminance level of 50.

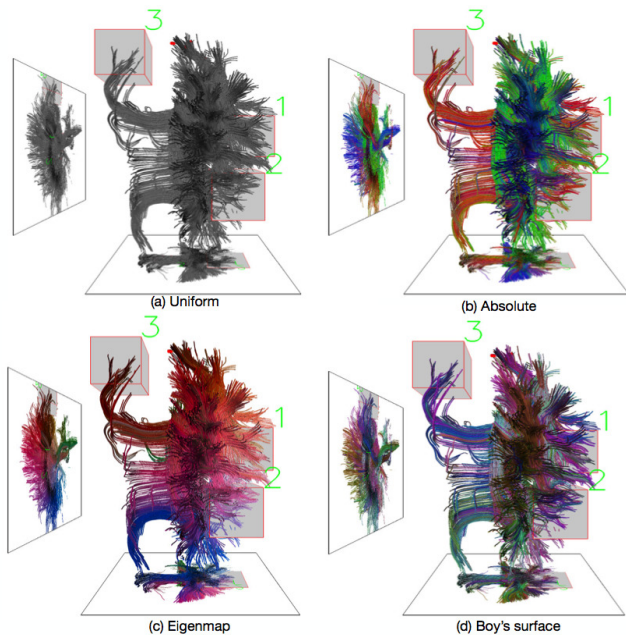


Fig. 4. Task 2's Four Orientation Colormaps

The *extended blackbody colormap* is a monotonic luminance colormap and adds blue and purple hues to the blackbody map described above with arc-length 200.

The *coolwarm colormap* has monotonically increased and decreased luminance. This colormap has the same luminance range and variations along the luminance direction as the diverging map; it adds yellow and cyan hues to the diverging map because these two hues are common transitions in coolwarm colormaps that use red and blue.

#### 4.3.2 Four Ensemble Direction Colormaps

The four spherical colormaps shown in Figure 4 are used in task 2 (ensemble tract tracing).

*Baseline uniform* is used as a control condition.

*Absolute RGB color-triples* uses Pajevic's approach [21] in which the three different orientations (left-right, dorsal-ventral, anterior-posterior) are represented as red (R), green (G), and blue (B). Each tract uses a constant color indicating its global orientation.

*Eigenmap embedding* implements the method of Brun et al. [66]. It assigns colors to tracts based on the similarities among tracts. The tracts become points in the embedded low-dimensional space [67] and the similarity of tracts is measured using the closeness of these points and a similarity matrix. The 3D coordinates of the points are normalized to fit into the displayable range of the  $L^*A^*B^*$  color space and the corresponding colors are used for the tracts.

The *Boy's surface embedding* implements the method of Demiralp et al. [22], a one-to-one mapping between an orientation and a location in a color space based on a Boy's surface immersion in the color space. The embedding is also *angular uniform*, i.e., the larger the difference in tract orientations, the larger the perceptual difference in their colors.

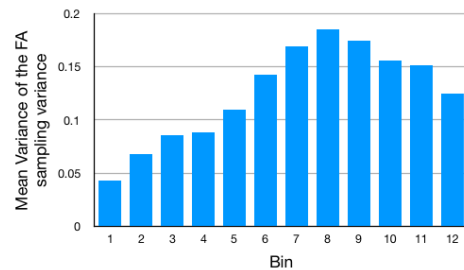


Fig. 5. Domain-Specific Data Attributes: The spreads (variances) of all AverageFA data in each of the 12 bins in our random samples, are smaller when AverageFA is in the lower bins and become most spread (with larger variances) when the bins ids  $\in [7, 9]$ . From bin 1 to bin 12, the average FAs are 1: [0.25, 0.3), 2: [0.3, 0.35), 3: [0.35, 0.4), ....., 12: [0.8, 0.85] respectively.

#### 4.4 Diffusion MRI Datasets

For task type 1, the average FA values are in the range [0.25, 0.85]. We evenly divided this range into 12 bins and the step size was 0.05. We randomly sampled within the four brain regions (here corpus callosum (CC), cortical spinal tracts (CST), inferior frontal occipital fasciculus (IFO), and inferior longitudinal occipitotemporal fasciculus (ILF)) by randomly placing boxes in these regions. We then take an equal number of samples in each bin from these samples. Fig. 5 shows the variance of the data in these 12 bins. We see that the lower and higher mean FA would have narrower spread (smaller variance) than those in the middle; this is the unique domain-specific data attribute.

Because ensemble mean is affected by variance [32], one way to conduct a study is to control the variance in each bin and measure the color effectiveness in each bin. We did not do this in order to retain a high-fidelity representation of tractography features; otherwise, we would have to produce artificial data to control the spread in each bin.

For task type 2, tractography data were computed from source DMRI images captured from a normal human brain at resolution  $0.9375mm \times 0.9375mm \times 4.52mm$ . Data are also sampled from four major bundles CC, CST, IFO, and ILF. All tracts are rendered using tubes.

#### 4.5 Experimental Design

Within-participant design was used for both tasks: i.e., each participant examined all colormaps. The independent variable is colormap. The dependent variables are completion time, accuracy, and subjective ratings. For task type 1 of ensemble average with 6 colormaps, each participant performed 12 instances (in each of the 12 bins) using each of the 6 maps (72 trials). Six instances of data (two CST, two CC, one ILF, and one IFO sample) and the six maps form a Latin square. No data was repetitively used by the same participant.

For task type 2 of the ensemble set using four colormaps, each participant performed eight instances of each coloring condition with four instances of each of the four bundles (32 trials). Again, datasets were not reused by the same participant. We ordered the four bundles and the four colormaps by a  $4 \times 4$  Latin square. The order of the trials for each colormap was randomized.

Each participant performed  $72 + 32 = 104$  sub-tasks.

#### 4.6 Participants, Apparatus, and Environment

A total of 24 participants (17 male and 7 female) took part in the study: two medical professionals, seven computer science students, and 15 students from other disciplines (mechanical engineering, math, and global studies). Their average age was 27.8 years with standard deviation 4.0. All participants had normal or corrected-to-normal vision and normal color vision tested using Ishihara Color Test.

The program runs on a Linux desktop with a 27" monitor (BenQ GTG XL 2720Z, resolution 1920 × 1080). Gamma was adjusted daily to ensure uniform perceived brightness: the gamma value used for the display was 2.2.

The lighting used fixed-pipeline OpenGL rendering with per-vertex lighting and Gouraud shading. We used a traditional three-point lighting scheme. Key and fill lights were placed in relation to a preset camera with 35mm focal length and the key light is at the top left of the scene, the location assumed by most human observers. Lighting placement and intensity are chosen to generate images with contrast and lighting properties appropriate for the data and human assumptions. For example, the key and fill lights are elevated and slightly to the left and right of the observer. All lights were white. The screen background color was white.

#### 4.7 Procedure

Participants were tested for normal vision and passed the Ishihara Color Vision test. They received general information about brain structure and about DMRI techniques and their medical uses. The training session, which lasted about 15 minutes, ensured that the participants understood the coloring and tasks.

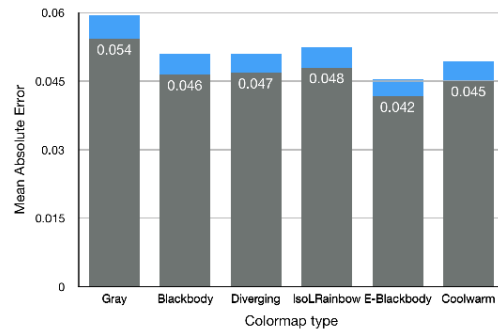
Task completion time was recorded from the time when the visualization was shown on the screen to the time when the final answer button was clicked. Participants were told to be as accurate and as fast as possible, and that accuracy was more important than time. They were also told to rotate the data to better interpret the structures. They had to finish a task in order to go to the next one. No time limit was set on each task. They could take a break at any time. After finishing all sub-tasks using each colormap, they selected from a 7-point scale (1 (worst) to 7 (best)) on the computer screen to rate the map they just used. Finally, participants were interviewed for their comments. Participants took about an hour on average to finish this study and received monetary compensation. No fatigue was reported.

We conducted three pilot studies comparing performance with a total of 50 participants (including 3 brain scientists) to refine our experimental procedure. These pilot study participants were not used in the formal study. We recruited brain scientists to collect some domain-specific comments related to brain sciences on the color encoding methods. The main difference between expert and novice groups, as observed in our previous study and the pilot studies, was that experts took longer to complete task because they were more interested in examining the data. Our pilot studies revealed no significant difference in task completion time and accuracy between medical school students and other college students without medical backgrounds.

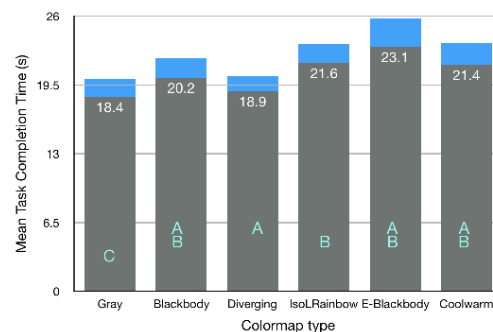
TABLE 1

Main Effects of Colormap on Accuracy and Task Completion Time and Effect Size. Here C stands for color and P for participant. The *large* effect sizes are in **bold** and the medium ones in *italic*.

Average	C on error	$F(5, 1728)=0.98, p=0.43$	$d=0.16$
	C on time	$F(5, 1728)=6.23, p<0.0001$	$d=0.31$
	P on error	$F(23, 1728)=2.77, p<0.0001$	$d=0.71$
	P on time	$F(23, 1728)=50.24, p<0.0001$	$d=3.72$
Orientation	C on error	$\chi^2(3, 768)=13.94, p=0.0030$	$V=0.13$
	C on time	$\chi^2(3, 768)=6.67, p=0.57$	$d=0.13$
	P on error	$\chi^2(23, 768)=23.47, p=0.43$	$V=0.17$
	P on time	$\chi^2(23, 768)=4.35, p<0.0001$	$d=1.56$



(a) Absolute Error



(b) Absolute Task Completion Time

Fig. 6. Task 1: Mean Absolute Error and Task Completion Time. The blue bars show 95% confidence intervals. (A). *Absolute error* =  $|participant's\ answer - ground\ truth|$ . (B). Colormaps labeled with the same cyan letter belong to the same group in the post-hoc analysis.

## 5 RESULTS

We collected 2496 data points with 24 participants for the two ensemble tasks, or 1728 and 768 for the *ensemble average* and *ensemble set* tasks accordingly. To summarize, the first hypothesis (H1 on rainbow) is partially supported. H2 on multihue, H3 on gray, and H5 on colorfulness are supported. We find no evidence to support H4 on resolution.

### 5.1 Overview of Analysis Approaches and Summary Statistics

Results were analyzed by tasks; Table 1 shows the statistical analysis of accuracy and task completion time measured using the following statistical approaches. For both tasks, we examine the main effect of colormap on error and task completion time using the SAS GLM procedure. A post-hoc analysis using the Tukey Studentized Range test (HSD) is performed when we observe significant main effects.

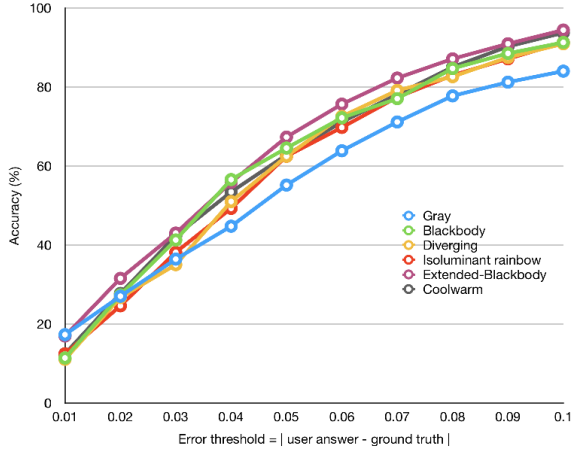


Fig. 7. Colormap Accuracy

Task 1 performance is analyzed using several methods. Task completion time is converted to  $\log_{10}$ -based to obtain a close-to-normal distribution. We compute error by the distance from the participants' answers to the ground truth and use the formula  $error = \log_2 |participant's\ answer - ground\ truth| + 8$ , following Cleveland and McGill [35]. We explore the accuracy of these ensemble colormaps using two additional measurements.

- Accuracy. Accuracy is percentage of correct answers. We threshold the error to measure whether an answer is correct. We used  $\delta = |participant's\ answer - ground\ truth|$  and threshold  $\delta$  to 0.01-0.04 with step size 0.01. An answer is considered correct when it falls in  $\delta$ .
- Directional Bias. We compute whether or not the colormaps bias observers towards values larger or smaller than ground truth.

The accuracy data in Task 2 are binary and are analyzed using logistic regression and reported using the  $p$  value from the Wald  $\chi^2$  test. When the  $p$  value is less than 0.05, variable levels with 95% confidence interval of pairwise difference of odds ratios not overlapping are considered significantly different. The  $\chi^2$  test with the "freq" procedure is used to examine whether or not there is a significant correlation between the main effect (the colormap or participant) and accuracy.

We measure effect sizes using Cohen's  $d$  for time and task type I error and Cramer's  $V$  for correctness to understand the practical significance [68]. We used Cohens benchmarks for "small"(0.07-0.21), "medium" (0.21-0.35), and "large" (> 0.35) effects.

### 5.2 Task 1 Ensemble Average Results

For task type 1, ensemble average, colormaps was not a significant main effect on error (Table 1 and Fig. 6(a)). A general trend was that extended blackbody had the least error and gray had the most.

Colormap and participant are significant main effects on time. (Table 1 and Figure 6(b)). The post-hoc analysis suggests three Tukey groups: (gray), (blackbody, isoluminant-rainbow, extended-blackbody, and coolwarm), and (blackbody, diverging, extended-blackbody, and coolwarm). The

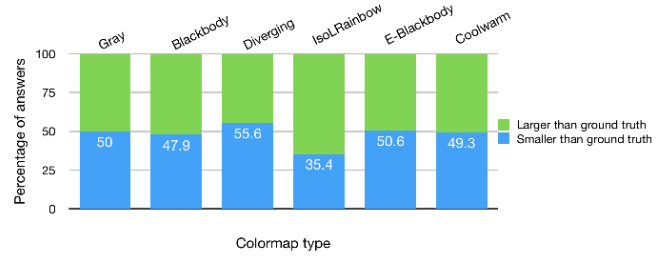


Fig. 8. Directional Biases by Colormap. More participants tend to overshoot (report larger than the ground truth) when using isoluminant rainbow. Using the diverging colormap, more participants underestimated the ensemble average. Gray, extended-blackbody, and coolwarm had the minimum directional biases.

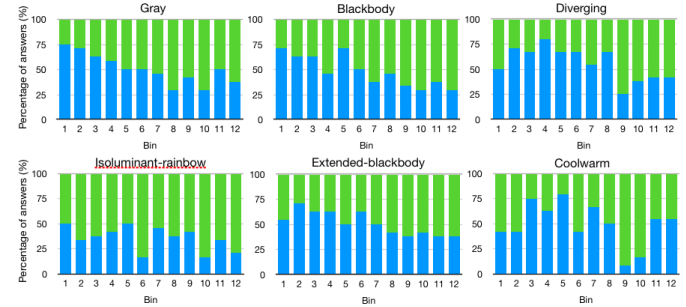


Fig. 9. Directional Biases by Colormap and Bin. More than 50% larger-than-ground-truth answers appeared in all 12 bins for isoluminant rainbow.

extended-blackbody and coolwarm maps led to the longest task completion time and the gray, though efficient, had the highest error.

### 5.3 Task 1 Color Sensitivity and Directional Bias

We compute the colormap sensitivity by measuring the percentage of correct answers or accuracy (Fig. 7). We first compute the mean absolute error. Fig. 7 showed that gray had on average the lowest accuracy among all colormaps.

Directional bias measures if observers consistently choose larger or smaller values than the ground truth using a colormap. We found that more answers using isoluminant rainbow were biased towards higher values, while the diverging color slightly towards lower answers (Fig. 8). All other colormaps of blackbody, extended-blackbody, and coolwarm showed about even distributions between higher and lower participants' answers.

We further analyzed the bias distribution in the 12 bins (Fig. 9). We found that more than 50% of the answers overshoot (selected larger than ground-truth) when using isoluminant-rainbow in all bins. Correlations between the data variance and colormap absolute error show that these two variables are statistically significantly correlated for all other maps except the isoluminant-rainbow. This result may indicate that the ensemble behaviors of isoluminant-rainbow might not be as predictable, despite its accuracy for ensemble average is comparable to other colormaps.

### 5.4 Task 2 Ensemble Spherical Colormap Results

The second row in Table 1 shows the statistical results. Fig. 10(a) shows mean accuracy (percentage correct an-



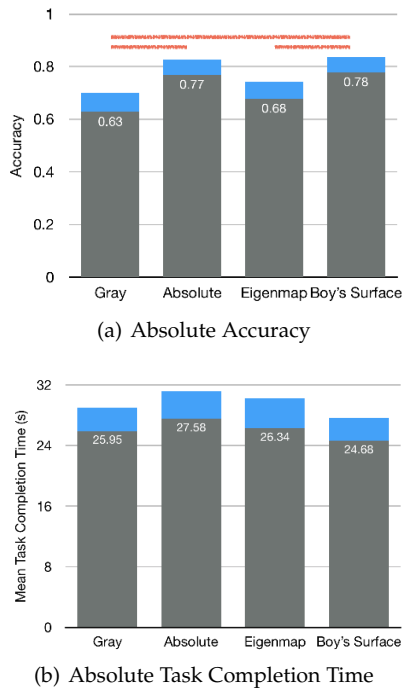


Fig. 10. Task 2: Mean Time and Accuracy. The color schemes connected by the orange line are significantly different.

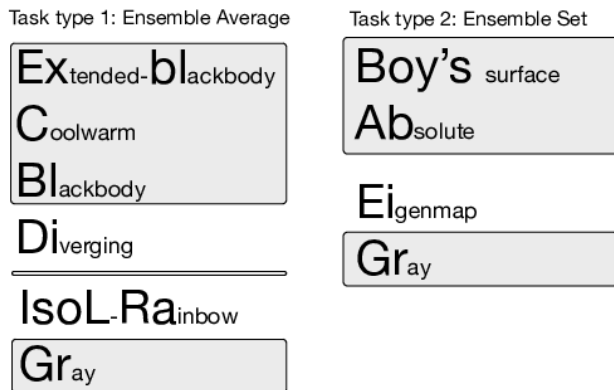


Fig. 11. Ensemble Ranking of Visualization Methods.

swers) and time and 95% confidence intervals from the mean. Colormap had a significant main effect on accuracy but not on task completion time. H4 is not supported. The Boy's surface embedding and the absolute embedding lead to most accurate answers for following tracts, followed by eigenmap. Boy's surface also shortened task completion time. This task does not require participants to utilize symmetry. The Boy's surface method was more accurate and also fast (Figs. 10(a) and 10(b)). It is also noticeable that the Boy's surface and absolute maps improved accuracy by 15% and 14% respectively compared to the baseline gray. Our results support the last hypothesis (colorfulness hypothesis) since all maps with colors increase accuracy over the gray baseline.

## 5.5 Subjective Ratings and Comments

Participants' ratings and comments provide useful insights into how the usefulness of the colormaps was perceived. Participants' subjective rating of the usefulness of these colormaps, from high to low are: task1: coolwarm (5), extended-blackbody (4.96), blackbody (4.96), diverging (4.75), isoluminant-rainbow (4.4), and grayscale (3.7); task2: absolute (5.3), eigenmap (5.3), Boy's surface (4.8), and uniform uniform-gray (2). Grayscale in task 1 and uniform gray with no coloring was rated least useful for both tasks.

The interviews revealed that those who liked the *absolute* method found it the simplest to understand and easiest for following the tracts because of its symmetry; in addition, the less chaotic color changes helped them recognize the orientations better. Those who disliked the absolute method thought that tracts looked too similar to differentiate, showing the tradeoffs between similarity and resolution. Most participants were relatively neutral on the *Boy's surface*, considering it similar to the *eigenmap* method in terms of hue uses (spatial resolution) despite including more hues than that method. Participants commented that "it (*Boy's surface*) was useful to have some different hues, but too many hues made the visualization less intuitive", while others stated that the "right amount of hues of *eigenmap* provided enough discriminations between values without overloading one's perception capability."

## 6 DISCUSSION

This section discusses our results. Fig. 11 shows our recommendations for choosing colormaps for the two ensemble tasks studied here.

### 6.1 Isoluminant Rainbow Does Not Decrease the Mean Accuracy, but Introduce Biases

Our first hypothesis is only partially supported. The most interesting result may be that the isoluminant rainbow does *not* introduce greater error on average for task 1 (Fig. 7). This efficiency result may agree with those in vision science because humans can average hues because humans can average hues [54]. However, none of the vision science studies to our knowledge drills down to the empirical study results to examine whether or not participants would be biased towards higher or lower than ground truth. The fact that isoluminant rainbow introduces higher overshooting needs to be further studied, perhaps by explicitly controlling the variance in data for us to learn the colormap behaviors. Rainbow colors are known to be poor for univariate encoding due to the lack of uniformity and ordering and because they produce artificial boundaries in data. We could conclude from our study that ensemble color processing differs from univariate colormap representations.

We do not recommend this isoluminant-rainbow map for ensemble average tasks. Instead, we propose to further explore *how* and *why* multihue works for limited capacity ensemble processing. This is mainly because the biases in isoluminant rainbow are consistent independent of the variances in data (Fig. 5 and Fig. 9). The rainbow map certainly uses a set of semantically meaningful colors that would ease human understanding and our brain scientist collaborators

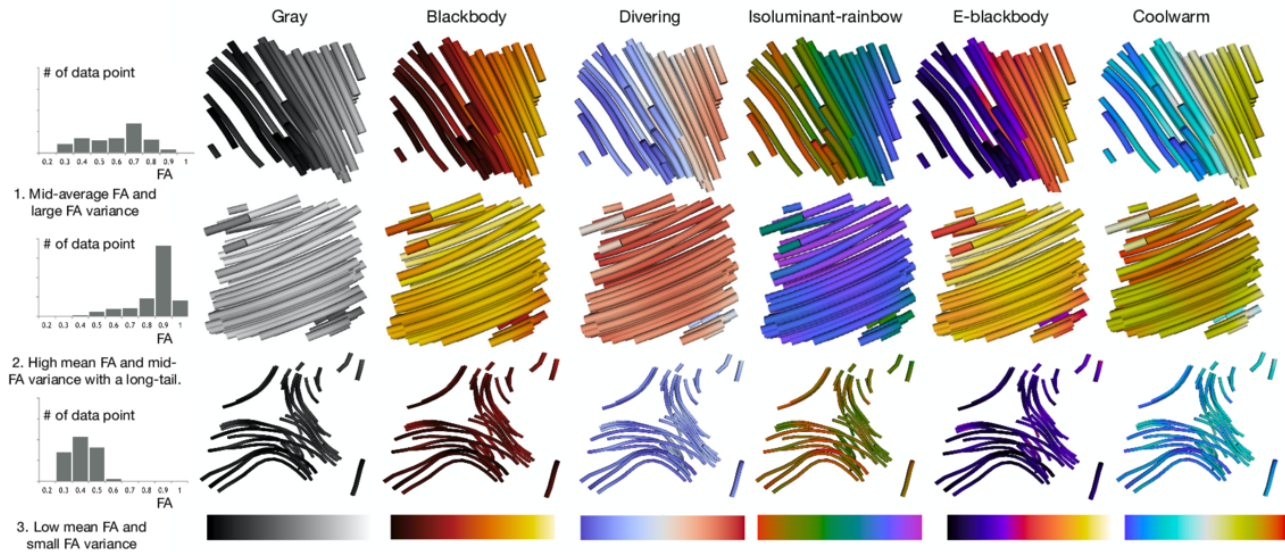


Fig. 12. Example Dataset Distribution and Their Colormaps: top: high-variance; middle: higher mean FA and narrow long-tail; bottom: low mean FA and narrow variance.

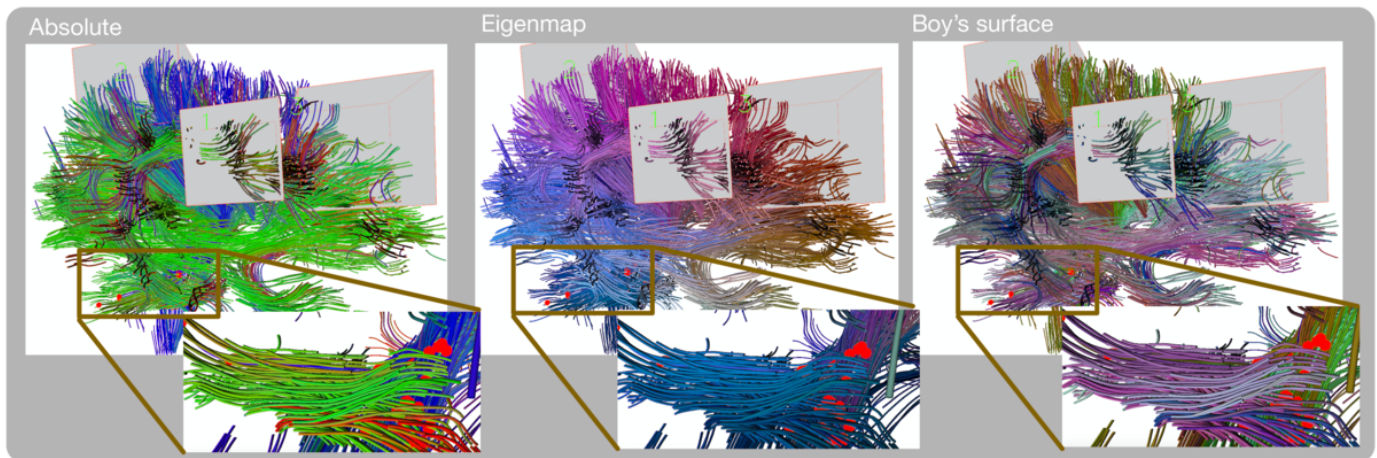


Fig. 13. An example from the empirical study for which all participants got correct answers using absolute and Boy's surface but only half the participants got correct answers with Eigenmap. Red dots in the subfigures are sources. Eigenmap tends to show similar colors in cases in which the other two methods produce visually distinguishable ones.

particularly love rainbows; however, rainbow maps may still violate Trumbo's color design heuristics that "the basic information should be displayed in a clear and logical fashion so that it may be decoded with precision and without continual references to the key (labeled scheme)" and "if small neighboring regions produce illusion of color over larger map areas, these illusions should not give misleading information" [44].

## 6.2 Multihue Maps Improve Ensemble Accuracy in General

Our second hypothesis about multihue efficiency is supported. We ran a statistical analysis to examine whether or not hue or luminance affect error or task completion time. We found that hue had a significant main effect on time ( $F(2, 1728) = 4.99, p = 0.0069$ ). The post-hoc analysis showed that colormaps with multihue led to statistically

significantly longer task completion time than single-hue (gray) colormaps.

The multihue extended-blackbody and the coolwarm colormaps had the lowest absolute error, with slightly longer task completion time. This accuracy result of extended-blackbody agrees with 2D study results as well, though we did not observe significant differences. There may be at least two reasons for the benefits. First, one might think these two colormaps had the largest arc-length and thus yielded slightly better results than other maps. The other, perhaps primary reason for the benefits is that the multihue lets participants quickly determine the target-region first before formulating their answers, and this two-stage viewing could also explain why rainbows also take longer to execute. Visual inspection of colormaps applied to empirical data in three different FA distributions (Fig. 12) shows the FA variances when the mean is around the mid-

dle (top row), in the higher (middle row) or lower (bottom row) end. We may observe that the colormaps in the last three columns with many hues may help viewers quickly locate the target regions on the colormap into which the answers fall.

### 6.3 That Many Colormaps Work Well Also Shows the Power of Human Visual Systems in Judging Ensemble Averages

We did not observe differences in accuracy among colormaps when measuring the distance of participants' answers from the ground truth. This result suggests the power of visual ensembles for quantitative estimates.

Balancing all considerations of efficiency, error, and correctness, and bias in these colormaps, we rank them in the order shown in Fig. 11 task 1, where extended-blackbody, coolwarm, and blackbody seem to work well. Isoluminant-rainbow and diverging are worth further investigations. Gray is not recommended because of their higher biases. Though we cannot say whether the poor performance of grayscale was caused by its simultaneous contrast or its sole luminance channel, the result indeed is in agreement with the literature on 2D colorization.

### 6.4 Local Contrast and Resolution Together Might Be the Most Decisive Property for Ensemble Direction Tracing

Our results present an uncanny valley effect where the highest and lowest resolution maps improved outcome compared to the mid-resolution eigenmap orientation map. H4 is not supported.

Overall, our results did not suggest that *resolution* contributes to higher accuracy in 3D space, since both the Boy's surface and absolute methods reduced errors. The eigenmap had reasonable resolution, as does the Boy's surface colormap, but lowered accuracy. To understand *when* Boy's surface and absolute succeeded and eigenmaps failed, we inspected qualitatively by the best and worst examples of participant accuracy when using these colormaps, as shown in Fig. 13. We see that, while eigenmap provides regional coloring, the adjacent regions have relatively low contrast compared to other two approaches. These observations may suggest that local contrast is the most decisive property, since a combination of high contrast and spatial resolution, as in the Boy's surface, led to higher accuracy on ensemble tracing. Boy's surface generates colors that seem to strike the right balance in the spatial resolution and contrast for this spatial structure determination. Finally, the data sample varies so no dataset is seen twice by the same participants. For the eigenmap, this setting means that the colors for the same tracts in different datasets would change, while the same tube would always be given the same color with the other maps.

We therefore recommend Boy's surface and absolute for coloring DMRI ensemble set, as shown in Fig 11.

### 6.5 Reuse of Our Results to Other Ensemble Representations

We sought to further our understanding of the ensemble data processing to generate concrete implications for visual

analysis of brain DMRI tractography datasets. In general, both tasks suggest that high-contrast localized colormaps may have helped both ensemble average and tract discrimination. Reuse of our results in other domains would have to take into account domain specificities of data, task, and user. Several areas could benefit from our work, such as weather forecasting [27], hurricane track prediction [69], and motion or movement trajectories [70] [71], because direct trajectory depiction has been informative. The most suitable reuse would be when the datasets have relatively low variance, so that colormaps can be localized to a smaller regions on a colormap for scalar data visualizations. Similarly, the spherical orientation colormap for line field visualizations might also be domain-dependent. In our case, the tracts are following three major orientations. We also did not consider other tract shapes. Considering appropriate distance measures is needed for maximal performance.

### 6.6 Participants' Experiences

Participants in this study have different backgrounds, and an ideal condition might be to use only brain scientists, clinicians, or medical school students. One major reason for the background differences was that we had access to only a few brain scientists. We used as many as possible in the study because we wanted to collect their comments related to the brain science domain.

Also, we followed Munzner's approach [55] of abstracting tasks into a level suitable for empirical study. In other words, these tasks could be performed by a trained participant. This may explain why we did not observe differences in task completion time and accuracy between students with and without medical backgrounds. Several user studies in flow visualization have used non-domain experts, suggesting that non-domain-expert is a viable option in empirical studies [72].

### 6.7 Using Ensemble for Visualization Design

It is intuitive to think that hue, due to its categorical effect (e.g. yellow or red), would interfere with the ensemble coloring, thus making representing a multihue average difficult. However, this turns out not to be the case. In vision science, ensemble is believed to be used by the human visual system to address our severely limited visual working memory. We can quickly derive patterns that guide our attention towards the most useful information. Scientific data is often highly structured and may carry redundant structures. When there is redundancy, it is possible to sample and filter to produce optimal views. For example, a handful of past visualization work has shown that implicit or explicit representation of sets of objects as groups or ensembles can guide observers' attention to process only the most relevant incoming information (e.g., explicit depiction of a group of objects in clusters [73], grouping interfaces to augment exploration workflows [74] [75] or using spatial patterns to form texture pattern to guide observers' behavior [38]). We believe there will be an opportunity to create a compressed and efficient ensemble representation of information, such as ensemble overviews, to guide visual attention to the areas more relevant to the targets.

## 6.8 Limitations and Future Work

The aim of this paper was to investigate the effect of coloring in practice on two spatial ensemble visualization tasks, average and set orientation. Our study is only a first step towards understanding ensemble tasks in visualizations. Although this study can suggest *what* colormap to choose for ensemble representation, we may need to build computational models or isolate factors (e.g., hue and luminance for task 1 and resolution and uniqueness for task 2) to explain *how* these colormaps are used by our visual system. Effectiveness of these coloring approaches needs to be studied further when tasks are related to other discrimination and detection tasks, in which quantitative differences among data are to be reported.

Our study would suggest further work. Since multihue colormaps in general improved ensemble average accuracy, one could run studies to systematically control the mean and variance of the ensemble datasets to model the ensemble performance. Viewers make a two-alternative forced-choice judgment about which visualization method contains the larger average value. Sensitivities are measured based on the differences between the values. A psychometric function fitted to the data reveals sensitivity to the discriminative threshold to measure accuracy. Using this method, we could answer questions about *why* and *when* multihue average will be effective and how variance influences the effectiveness and efficiency.

## 7 CONCLUSION

This study is the first (to our knowledge) to compare different color ensemble encodings for 3D DMRI tractography visualizations. Results from the study provide the following insights for choosing 3D tube coloring ensembles.

- The most interesting result was that the isoluminant-rainbow performed reasonably well, though it did lead to more reporting bias towards higher than ground truth values than other colormaps.
- Extended-blackbody, coolwarm, and blackbody are reasonably accurate for ensemble average in 3D. Our analysis showed that hue had much larger influence on error than luminance.
- Our study on the ensemble set orientation discrimination supports the proposition that having some colors is significantly better than no color at all.
- Colormaps with better orientation contrast (e.g., the Boy's surface and the absolute approach) are most desirable for ensemble set orientation discrimination tasks such as tract tracing.

## APPENDIX A

### THE UNIVARIATE COLORMAPS IN THE $L^*A^*B^*$ COLOR SPACE

Fig. 14 shows the scalar colormaps in the  $L^*A^*B^*$  color space. The curve in each figure shows the trajectory of color maps and their three projects in the  $L^*A^*B^*$  color space. All color interpolation is performed using linear interpolation in this space.

We used the Rogowitz-Kalvin [76] and Kindlmann-Reinhard-Creem approaches [39] to help visually inspect colormaps to test their luminance profile. This method utilizes our sensitivity to luminance variations in human faces to select colormaps. Fig. 15 shows samples of faces generated by these six colormaps with our online tool. The faces with isoluminance-rainbow and diverging colormaps are less recognizable than all others. The rainbow and coolwarm colormaps help distinguish different values: one can clearly see red (high) values around the nose and under the eyes.

## APPENDIX B

### COLORING TOOL WEBSITE

Our own tool (Fig. 16) is hosted at <http://wchiou1.github.io/colorTool/> (Fig. 16). During the evaluation process, we found that using a coloring tool to quickly provide side-by-side comparison made our discussion with the medical doctors very effective and efficient. The direct manipulation interface lets users directly drag and drop plain-text colormaps. It can display both 2D image and 3D geometry examples.

## ACKNOWLEDGMENTS

The authors would like to thank Drs. Peter Kochunov, L. Elliot Hong, and Neda Jahanshad for their discussions on color uses in brain science, Dr. Bernice Rogowitz for a discussion on colormap uses in real-world applications, Dr. Jeremy Wolfe for his thorough review and comments on this manuscript, and the anonymous reviewers for their constructive comments. The authors also thank the participants at University of Maryland, Baltimore County, University of Maryland Medical School, and Veterans Affairs Medical Center of Providence, RI for their time and effort. We thank Katrina Avery for her editorial support. This work was supported in part by NSF IIS-1302755, CNS-1531491, DBI-1260795, IIS-1018769, and DUE-0817106 and by NIST MSE-70NANB13H181. Any opinions, findings, and conclusions or recommendations expressed in this material are those of the authors and do not necessarily reflect the views of National Institute of Standards and Technology (NIST) or the National Science Foundation (NSF).

Jian Chen is the corresponding author.

## REFERENCES

- [1] M. N. Phadke, L. Pinto, F. Alabi, J. Harter, R. M. Taylor II, X. Wu, H. Petersen, S. A. Bass, and C. G. Healey, "Exploring ensemble visualization," in *Proceedings of SPIE*, vol. 8294, no. 82940B (12 pages), 2012.
- [2] A. Y. Leib, A. Kosovicheva, and D. Whitney, "Fast ensemble representations for abstract visual impressions," *Nature Communications*, vol. 7 (article number 13186), 2016.
- [3] A. Chetverikov, G. Campana, and Á. Kristjánsson, "Representing color ensembles," *Psychological Science*, vol. 28, no. 10, pp. 1510–1517, 2017.
- [4] D. Ariely, "Seeing sets: Representation by statistical properties," *Psychological Science*, vol. 12, no. 2, pp. 157–162, 2001.
- [5] N. Robitaille and I. M. Harris, "When more is less: Extraction of summary statistics benefits from larger sets," *Journal of Vision*, vol. 11, no. 12, pp. 1–8, 2011.

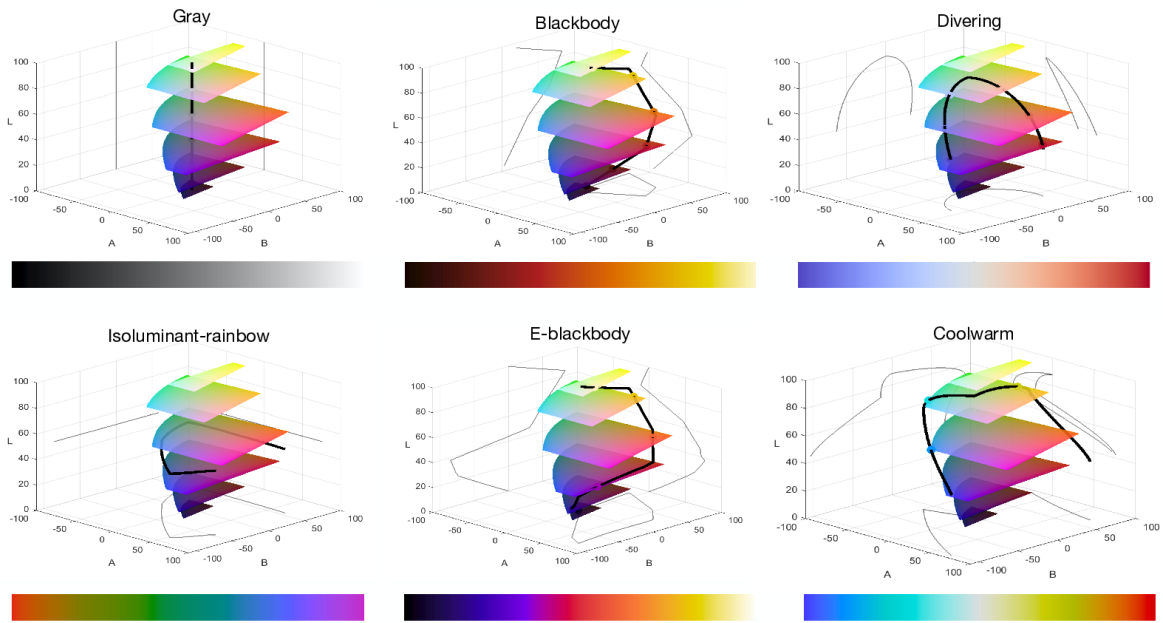


Fig. 14. Colormap Profile for Showing Scalars in Task 1 (AverageFA tasks) in the  $L^*A^*B^*$  color space. L-planes from bottom to top are  $L=5, 20, 40, 60, 80,$  and  $95$ .

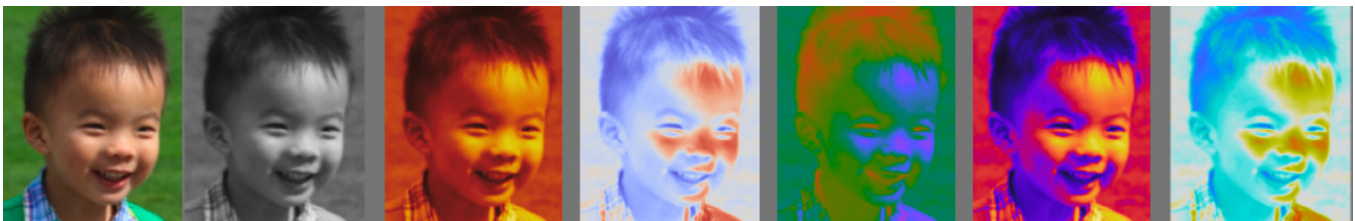


Fig. 15. Using Faces to Examine the Luminance Profile of Colormaps (from left to right): original image, gray, blackbody, diverging, isoluminant-rainbow, extended-blackbody, and coolwarm colormaps.

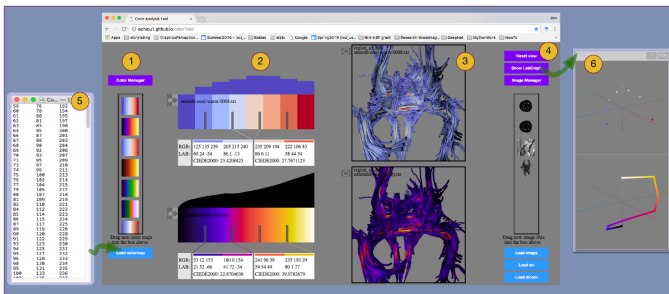


Fig. 16. Exploratory Color Comparison Tool.

[6] G. A. Alvarez and A. Oliva, "The representation of simple ensemble visual features outside the focus of attention," *Psychological Science*, vol. 19, no. 4, pp. 392–398, 2008.

[7] D. W. Williams and R. Sekuler, "Coherent global motion percepts from stochastic local motions," *Vision Research*, vol. 24, no. 1, pp. 55–62, 1984.

[8] S. N. Watamaniuk and A. Duchon, "The human visual system averages speed information," *Vision Research*, vol. 32, no. 5, pp. 931–941, 1992.

[9] D. Burr and J. Ross, "A visual sense of number," *Current Biology*, vol. 18, no. 6, pp. 425–428, 2008.

[10] M. F. Neumann, S. R. Schweinberger, and A. M. Burton, "Viewers extract mean and individual identity from sets of famous faces,"

*Cognition*, vol. 128, no. 1, pp. 56–63, 2013.

[11] A. Oliva and A. Torralba, "Building the GIST of a scene: The role of global image features in recognition," *Progress in Brain Research*, vol. 155, pp. 23–36, 2006.

[12] B. Bauer, "Does Stevens's power law for brightness extend to perceptual brightness averaging?" *The Psychological Record*, vol. 59, no. 2, p. 171, 2009.

[13] T. C. Chua, W. Wen, M. J. Slavin, and P. S. Sachdev, "Diffusion tensor imaging in mild cognitive impairment and Alzheimer's disease: a review," *Current Opinion in Neurology*, vol. 21, no. 1, pp. 83–92, 2008.

[14] L. Zhou and C. D. Hansen, "A survey of colormaps in visualization," *IEEE Transactions on Visualization and Computer Graphics*, vol. 22, no. 8, pp. 2051–2069, 2016.

[15] S. Silva, B. S. Santos, and J. Madeira, "Using color in visualization: A survey," *Computers & Graphics*, vol. 35, no. 2, pp. 320–333, 2011.

[16] G. D. Finlayson, S. D. Hordley, and P. M. Hubel, "Color by correlation: A simple, unifying framework for color constancy," *IEEE Transactions on Pattern Analysis and Machine Intelligence*, vol. 23, no. 11, pp. 1209–1221, 2001.

[17] M. H. Kim, T. Weyrich, and J. Kautz, "Modeling human color perception under extended luminance levels," in *ACM SIGGRAPH*, vol. 28, no. 3 (10 pages), 2009.

[18] K. Moreland, "Why we use bad color maps and what you can do about it," *Electronic Imaging*, vol. 2016, no. 16, pp. 1–6, 2016.

[19] M. Christen, D. A. Vitacco, L. Huber, J. Harboe, S. I. Fabrikant, and P. Brugger, "Colorful brains: 14 years of display practice in functional neuroimaging," *NeuroImage*, vol. 73, pp. 30–39, 2013.

[20] D. A. Szafir, S. Haroz, M. Gleicher, and S. Franconeri, "Four types of ensemble coding in data visualizations," *Journal of Vision*,

- vol. 16, no. 5, pp. 1–19, 2016.
- [21] S. Pajevic, C. Pierpaoli *et al.*, “Color schemes to represent the orientation of anisotropic tissues from diffusion tensor data: application to white matter fiber tract mapping in the human brain,” *Magnetic Resonance in Medicine*, vol. 42, no. 3, pp. 526–540, 1999.
- [22] C. Demiralp, J. F. Hughes, and D. H. Laidlaw, “Coloring 3D line fields using boy’s real projective plane immersion,” *IEEE Transactions on Visualization and Computer Graphics*, vol. 15, no. 6, pp. 1457–1464, 2009.
- [23] K. Potter, A. Wilson, P.-T. Bremer, D. Williams, C. Doutriaux, V. Pascucci, and C. R. Johnson, “Ensemble-vis: A framework for the statistical visualization of ensemble data,” in *IEEE International Conference on Data Mining Workshops*, 2009, pp. 233–240.
- [24] D. Whitney and A. Y. Leib, “Ensemble perception,” *Annual Review of Psychology*, vol. 69, no. 12, pp. 1–25, 2017.
- [25] G. A. Alvarez, “Representing multiple objects as an ensemble enhances visual cognition,” *Trends in cognitive sciences*, vol. 15, no. 3, pp. 122–131, 2011.
- [26] K. Potter, P. Rosen, and C. Johnson, “From quantification to visualization: A taxonomy of uncertainty visualization approaches,” *Uncertainty Quantification in Scientific Computing*, pp. 226–249, 2012.
- [27] J. Sanyal, S. Zhang, J. Dyer, A. Mercer, P. Amburn, and R. Moorhead, “Noodles: A tool for visualization of numerical weather model ensemble uncertainty,” *IEEE Transactions on Visualization and Computer Graphics*, vol. 16, no. 6, pp. 1421–1430, 2010.
- [28] R. S. Laramée, H. Hauser, H. Doleisch, B. Vrolijk, F. H. Post, and D. Weiskopf, “The state of the art in flow visualization: Dense and texture-based techniques,” in *Computer Graphics Forum*, vol. 23, no. 2, 2004, pp. 203–221.
- [29] N. Max, P. Hanrahan, and R. Crawfis, “Area and volume coherence for efficient visualization of 3d scalar functions,” *Proceedings of the Workshop on Volume visualization*, pp. 27–33, 1990.
- [30] A. Forsberg, J. Chen, and D. H. Laidlaw, “Comparing 3D vector field visualization methods: A user study,” *IEEE Transactions on Visualization and Computer Graphics*, vol. 15, no. 6, pp. 1219–1226, 2009.
- [31] J. Haberman and D. Whitney, “Ensemble perception: Summarizing the scene and broadening the limits of visual processing,” *From Perception to Consciousness: Searching with Anne Treisman*, pp. 339–349, 2012.
- [32] J. Maule and A. Franklin, “Effects of ensemble complexity and perceptual similarity on rapid averaging of hue,” *Journal of vision*, vol. 15, no. 4, pp. 6–6, 2015.
- [33] J. Haberman, T. F. Brady, and G. A. Alvarez, “Individual differences in ensemble perception reveal multiple, independent levels of ensemble representation,” *Journal of Experimental Psychology: General*, vol. 144, no. 2, pp. 432–446, 2015.
- [34] M. Correll, D. Albers, S. Franconeri, and M. Gleicher, “Comparing averages in time series data,” in *Proceedings of ACM SIGCHI*, 2012, pp. 1095–1104.
- [35] W. S. Cleveland and R. McGill, “Graphical perception: Theory, experimentation, and application to the development of graphical methods,” *Journal of the American statistical Association*, vol. 79, no. 387, pp. 531–554, 1984.
- [36] J. Webster, P. Kay, and M. A. Webster, “Perceiving the average hue of color arrays,” *JOSA A*, vol. 31, no. 4, pp. A283–A292, 2014.
- [37] O. Wright, C. Biggam, C. Hough, C. Kay, and D. Simmons, “Effects of stimulus range on color categorization,” *New directions in colour studies. Amsterdam: John Benjamin*, pp. 265–276, 2011.
- [38] H. Zhao and J. Chen, “Bivariate separable-dimension glyphs can improve visual analysis of holistic features,” *arXiv: https://arxiv.org/abs/1712.02333v1*, 2017.
- [39] G. Kindlmann, E. Reinhard, and S. Creem, “Face-based luminance matching for perceptual colormap generation,” in *Proceedings of the Conference on Visualization*, 2002, pp. 299–306.
- [40] G. Hu, Z. Pan, M. Zhang, D. Chen, W. Yang, and J. Chen, “An interactive method for generating harmonious color schemes,” *Color Research & Application*, vol. 39, no. 1, pp. 70–78, 2014.
- [41] C. C. Gramazio, D. H. Laidlaw, and K. B. Schloss, “Colorgorgical: Creating discriminable and preferable color palettes for information visualization,” *IEEE Transactions on Visualization and Computer Graphics*, vol. 23, no. 1, pp. 521–530, 2017.
- [42] R. Bujack, T. L. Turton, F. Samsel, C. Ware, D. H. Rogers, and J. Ahrens, “The good, the bad, and the ugly: A theoretical framework for the assessment of continuous colormaps,” *IEEE Transactions on Visualization and Computer Graphics*, vol. 1, no. 1, pp. 923–933, 2018.
- [43] D. A. Szafrir, “Modeling color difference for visualization design,” *IEEE Transactions on Visualization and Computer Graphics*, vol. 24, no. 1, pp. 392–401, 2018.
- [44] B. E. Trumbo, “A theory for coloring bivariate statistical maps,” *The American Statistician*, vol. 35, no. 4, pp. 220–226, 1981.
- [45] C. Ware, T. L. Turton, F. Samsel, R. Bujack, D. H. Rogers, K. Lamm, N. Smit, and D. Cunningham, “Evaluating the perceptual uniformity of color sequences for feature discrimination,” in *EuroVis Workshop on Reproducibility, Verification, and Validation in Visualization (EuroRV3)*. The Eurographics Association, 2017.
- [46] D. Penney, J. Chen, and D. H. Laidlaw, “Effects of illumination, texture, and motion on task performance in 3d tensor-field streamtube visualizations,” in *IEEE Pacific Visualization Symposium*, 2012, pp. 97–104.
- [47] H. Zhao, G. W. Bryant, W. Griffin, J. E. Terrill, and J. Chen, “Validation of splitvectors encoding for quantitative visualization of large-magnitude-range vector fields,” *IEEE Transactions on Visualization and Computer Graphics*, vol. 23, no. 6, pp. 1691–1705, 2017.
- [48] F. Ritter, C. Hansen, V. Dicken, O. Konrad, B. Preim, and H.-O. Peitgen, “Real-time illustration of vascular structures,” *IEEE Transactions on Visualization and Computer Graphics*, vol. 12, no. 5, pp. 877–884, 2006.
- [49] P. Svetachov, M. H. Everts, and T. Isenberg, “DTI in context: illustrating brain fiber tracts in situ,” in *Computer Graphics Forum*, vol. 29, no. 3, 2010, pp. 1023–1032.
- [50] D. Acevedo and D. Laidlaw, “Subjective quantification of perceptual interactions among some 2d scientific visualization methods,” *IEEE Transactions on Visualization and Computer Graphics*, vol. 12, no. 5, pp. 1133–1140, 2006.
- [51] M. Borkin, K. Gajos, A. Peters, D. Mitsouras, S. Melchionna, F. Rybicki, C. Feldman, and H. Pfister, “Evaluation of artery visualizations for heart disease diagnosis,” *IEEE Transactions on Visualization and Computer Graphics*, vol. 17, no. 12, pp. 2479–2488, 2011.
- [52] J. Chen, H. Cai, A. P. Auchus, and D. H. Laidlaw, “Effects of stereo and screen size on the legibility of three-dimensional streamtube visualization,” *IEEE Transactions on Visualization and Computer Graphics*, vol. 18, no. 12, pp. 2130–2139, 2012.
- [53] G. Kindlmann and D. Weinstein, “Hue-balls and lit-tensors for direct volume rendering of diffusion tensor fields,” in *Proceedings of the Conference on Visualization*, 1999, pp. 183–189.
- [54] J. Maule, C. Witzel, and A. Franklin, “Getting the gist of multiple hues: metric and categorical effects on ensemble perception of hue,” *Journal of the Optical Society of America. A, Optics, Image Science, and Vision*, vol. 31, no. 4, pp. A93–102, 2014.
- [55] T. Munzner, “A nested model for visualization design and validation,” *IEEE Transactions on Visualization and Computer Graphics*, vol. 15, no. 6, pp. 921–928, 2009.
- [56] S. Mori and J. Zhang, “Principles of diffusion tensor imaging and its applications to basic neuroscience research,” *Neuron*, vol. 51, no. 5, pp. 527–539, 2006.
- [57] C. Zhang, M. Caan, T. Höllt, E. Eisemann, and A. Vilanova, “Overview+ detail visualization for ensembles of diffusion tensors,” in *Computer Graphics Forum*, vol. 36, no. 3, 2017, pp. 121–132.
- [58] T. Isenberg, P. Isenberg, J. Chen, M. Sedlmair, and T. Möller, “A systematic review on the practice of evaluating visualization,” *IEEE Transactions on Visualization and Computer Graphics*, vol. 19, no. 12, pp. 2818–2827, 2013.
- [59] B. Preim, A. Baer, D. Cunningham, T. Isenberg, and T. Ropinski, “A survey of perceptually motivated 3D visualization of medical image data,” in *Computer Graphics Forum*, vol. 35, no. 3. Wiley Online Library, 2016, pp. 501–525.
- [60] P. Kochunov, H. Ganjgahi, A. Winkler, S. Kelly, D. K. Shukla, X. Du, N. Jahanshad, L. Rowland, H. Sampath, B. Patel, P. O’Donnell, Z. Xie, S. A. Paciga, C. R. Schubert, J. Chen, G. Zhang, P. M. Thompson, T. E. Nichols, and H. L. Elliot, “Heterochronicity of white matter development and aging explains regional patient control differences in schizophrenia,” *Human Brain Mapping*, vol. 37, no. 12, pp. 4673–4688, 2016.
- [61] S. Zhang, C. Demiralp, and D. H. Laidlaw, “Visualizing diffusion tensor MR images using streamtubes and streamsurfaces,” *IEEE Transactions on Visualization and Computer Graphics*, vol. 9, no. 4, pp. 454–462, 2003.
- [62] H. Jiang, P. C. van Zijl, J. Kim, G. D. Pearlson, and S. Mori, “DtiStudio: resource program for diffusion tensor computation and fiber bundle tracking,” *Computer Methods and Programs in Biomedicine*, vol. 81, no. 2, pp. 106–116, 2006.

- [63] S. Pieper, M. Halle, and R. Kikinis, "3D slicer," in *IEEE International Symposium on Biomedical Imaging: Nano to Macro*, 2004, pp. 632–635.
- [64] R. Borgo, J. Dearden, and M. W. Jones, "Order of magnitude markers: An empirical study on large magnitude number detection," *IEEE Transactions on Visualization and Computer Graphics*, vol. 20, no. 12, pp. 2261–2270, 2014.
- [65] G. Sharma, W. Wu, and E. N. Dalal, "The CIEDE2000 color-difference formula: Implementation notes, supplementary test data, and mathematical observations," *Color Research & Application*, vol. 30, no. 1, pp. 21–30, 2005.
- [66] A. Brun, H.-J. Park, H. Knutsson, and C.-F. Westin, "Coloring of DT-MRI fiber traces using laplacian eigenmaps," in *International Conference on Computer Aided Systems Theory*, 2003, pp. 518–529.
- [67] M. Belkin and P. Niyogi, "Laplacian eigenmaps for dimensionality reduction and data representation," *Neural Computation*, vol. 15, no. 6, pp. 1373–1396, 2003.
- [68] J. Cohen, *Statistical power analysis for the behavioral sciences*. New York: Academic Press, 1988.
- [69] J. Cox and M. Lindell, "Visualizing uncertainty in predicted hurricane tracks," *International Journal for Uncertainty Quantification*, vol. 3, no. 2, 2013.
- [70] J. Chen, M. Kostandov, I. Pivkin, D. Riskin, D. Willis, S. Swartz, and D. Laidlaw, "Visual analysis of dimensionality reduction for exploring bat flight kinematics in a virtual environment," in *Proceedings of the 15th Joint virtual reality Eurographics conference on Virtual Environments*. Eurographics Association, 2009, pp. 77–84.
- [71] N. Andrienko, G. Andrienko, and S. Rinzivillo, "Leveraging spatial abstraction in traffic analysis and forecasting with visual analytics," *Information Systems*, vol. 57, pp. 172–194, 2016.
- [72] Z. Liu, S. Cai, J. E. Swan, R. J. Moorhead, J. P. Martin, and T. Jankun-Kelly, "A 2D flow visualization user study using explicit flow synthesis and implicit task design," *IEEE Transactions on Visualization and Computer Graphics*, vol. 18, no. 5, pp. 783–796, 2012.
- [73] Z. Peng, E. Grundy, R. S. Laramée, G. Chen, and N. Croft, "Mesh-driven vector field clustering and visualization: An image-based approach," *IEEE Transactions on Visualization and Computer Graphics*, vol. 18, no. 2, pp. 283–298, 2012.
- [74] G. Li, A. C. Bragdon, Z. Pan, M. Zhang, S. M. Swartz, D. H. Laidlaw, C. Zhang, H. Liu, and J. Chen, "Visbubbles: a workflow-driven framework for scientific data analysis of time-varying biological datasets," in *ACM SIGGRAPH Asia Posters*, 2011, p. 27.
- [75] E. D. Ragan, A. Endert, J. Sanyal, and J. Chen, "Characterizing provenance in visualization and data analysis: an organizational framework of provenance types and purposes," *IEEE Transactions on Visualization and Computer Graphics*, vol. 22, no. 1, pp. 31–40, 2016.
- [76] B. E. Rogowitz and A. D. Kalvin, "The "which blair project": a quick visual method for evaluating perceptual color maps," in *Proceedings of the Conference on Visualization*, 2001, pp. 183–556.



**Guohao Zhang** is a PhD student in the Department of Computer Science and Electrical Engineering at University of Maryland, Baltimore County. He received his B.E. degree in Engineering Physics from Tsinghua University in 2012. His research interests include design and evaluation of visualization techniques and 3D visualizations. He is a student member of IEEE.



**Wesley Chiou** is an undergraduate student in the Department of Computer Science and Electrical Engineering at University of Maryland, Baltimore County. His research interest is human-computer interaction and visualization.



**David H. Laidlaw** received the PhD degree in computer science from the California Institute of Technology, where he also did post-doctoral work in the Division of Biology. He is a professor in the Computer Science Department at Brown University. His research centers on applications of visualization, modeling, computer graphics, and computer science to other scientific disciplines. He is a fellow of IEEE.



member of the IEEE and the IEEE Computer Society.

**Jian Chen** received the PhD degree in Computer Science from Virginia Polytechnic Institute and State University (Virginia Tech). She did her post-doctoral work in the Department of Computer Science at Brown University. She is an Associate Professor in Computer Science and Electrical Engineering at The Ohio State University where she directs the Interactive Visual Computing Laboratory (IVCL). Her research interests include design and evaluation of visualization techniques and virtual reality. She is a



search interests are in neuroimaging biomarkers for Alzheimer's disease and other dementias.

**Alexander P. Auchus** Dr. Alexander P. Auchus holds degrees from Johns Hopkins University and from Washington University in St. Louis. He is an elected fellow of the American Neurological Association, the American Academy of Neurology, and the American Geriatrics Society. He has served on the faculty of Emory University, Case Western Reserve University, and University of Tennessee. His present position is Professor and McCarty Chair of Neurology at the University of Mississippi Medical Center. Dr. Auchus's